Journal of Catalysis **182,** 463–469 (1999)
Article ID jcat.1998.2367, available online at http://www.idealibrary.com on IDEAL®

The Catalytic Performance of 14-Membered Ring Zeolites

J. Martinez-Triguero,* M. J. Diaz-Cabañas,* M. A. Camblor,* V. Fornés,*
Th. L. M. Maesen,† and A. Corma*,[1]

*Instituto de Tecnología Química (U.P.V.-C.S.I.C.), Universidad Politécnica de Valencia, Avenida los Naranjos, s/n, 46022 Valencia, Spain; and †PQ R&D Center, Zeolyst International, Conshohocken, Pennsylvania 19428-2240

Received August 18, 1998; revised November 26, 1998; accepted November 26, 1998

We have synthesized and carried out extensive characterization (IR, MAS NMR, TPD, Ar and N_2 adsorption, and scanning electron microscopy) of two unidirectional 14-membered ring zeolites (CIT-5 and UTD-1) and one unidirectional 12-membered ring zeolite (SSZ-24). All three samples have comparable acidic properties and are of comparable crystal size. The performance of these three zeolite samples in the catalytic cracking of *n*-decane, triisopropylbenzene, and a complex industrial feed (vacuum gas oil) have been evaluated. The performance of CIT-5, a 14-membered ring zeolite, is indistinguishable from that of SSZ-24, a 12-membered ring zeolite. A large, flat molecule—such as triisopropylbenzene—can be converted inside the 14-membered ring channels of a UTD-1 zeolite, but not inside the pores of CIT-5 or SSZ-24. In the catalytic cracking of complex feedstock, all three of the unidirectional zeolites are inferior in performance to the conventional tridirectional zeolites, such as USY or Beta zeolites.

INTRODUCTION

Microporous molecular sieves are used advantageously as acid, base, and redox catalysts (1). The use of novel organic cations in the synthesis of zeolites has yielded many new zeolite topologies (2). These include uni- and tridirectional 12-membered ring (MR) pores and 10 MR pores, and—more recently—topologies comprising a combination of both the 10 and the 12 MR pores (1, 2). Accordingly, there is now a rich gamut of zeolite topologies that can be used for fine-tuning shape selectively catalyzed reactions involving molecules with a diameter smaller than 0.8 nm. However, reactants with a diameter larger than 0.8 nm cannot diffuse into the pores of these zeolites and, hence, cannot be shape-selectively processed. Therefore, there has been a significant effort to synthesize zeolites with pores larger than 0.8 nm.

Molecular sieves such as cloverite (3) and cacoxenite (4) with pore sizes significantly larger than 0.8 nm are known. Thus far, these are of limited practical importance because their limited thermal stability and acidity preclude their use in catalysis.

[1] To whom correspondence should be addressed.

Very recently, two new high-silica zeolites were synthesized that contain unidirectional 14 MR channels. They were referred to as UTD-1 (5) and CIT-5 (6). UTD-1 was prepared by a hydrothermal synthesis using either bis (pentamethylcyclopentadienyl) cobalt (III) hydroxide or bis (tetramethylcyclopentadienyl) cobalt (III) hydroxide. UTD-1 has unidirectional 14 MR elliptical channels that are 0.75×1 nm in diameter (7). CIT-5 was synthesized under hydrothermal conditions using N(16)–methylspartenium hydroxide. The CIT-5 structure has unidirectional 14 MR channels with a diameter of 0.73 nm (8).

Thus far, only a limited number of catalytic experiments using UTD-1 or CIT-5 have been reported. These have failed to establish the potential benefits of the large pores of UTD-1 and CIT-5 for processing large molecules. In this paper we evaluate the catalytic potential of the novel unidirectional 14 MR structures and compare them with selected 12 MR structures.

EXPERIMENTAL

Materials

A SSZ-24-type zeolite was prepared by first synthesizing the borosilicate and subsequently substituting the framework boron by aluminum (9). Then 2.71 g of $Na_2B_4O_7$, $10H_2O$ was dissolved in 97.12 g of water. Next, 1.71 g NaBr and 60.51 g of a 0.55 M solution of N(16)–methylsparteinium hydroxide were added. Once a clear solution had been obtained, 10 g amorphous silica (Aerosil 200, Degussa) was added, and the mixture was stirred vigorously. This yielded a gel that was transferred to 60-ml teflon lined stainless steel autoclaves and heated at 448 K under slow rotation (60 rpm) for 10 days. After filtration, washing, and drying at 373 K, the solid product was calcined at 853 K for 3 h. This resultant SSZ-24 borosilicate was converted to a SSZ-24 zeolite by a contact with 50 ml/g of a 10 wt% aqueous solution of $Al(NO_3)_3$ at 373 K for 48 h. After filtration, washing, and drying, the solid was calcined at 773 K for 3 h.

CIT-5 zeolite was synthesized in a fluoride medium (8). Then 8.91 g of tetraethylorthosilicate and 0.23 g of

0021-9517/99 $30.00

aluminum isopropoxide were hydrolyzed in 27.02 g of a 0.823 M solution of N(16)–methylsparteinium hydroxide. The mixture was stirred vigorously in an open vessel to evaporate water and most of the alcohol until the H_2O/SiO_2 molar ratio was 15. Then, 0.91 g of a 46.9 wt% aqueous HF solution and 0.13 g all silica CIT-5 (8) seeds (suspended in 3 g of water) were added. After additional homogenization, the gel (molar composition SiO_2 : 0.013, Al_2O_3 : 0.52, *R*OH : 0.50, HF : 15 and H_2O where *R* is N(16)–methylsparteinium) was heated for 14 days in a Teflon-lined stainless-steel autoclave at 448 K under slow rotation (60 rpm). After filtration and washing, the recovered solids were dried at 373 K and calcined at 923 K for 3 h.

A UTD-1 borosilicate was synthesized by dissolving 0.67 g of H_3BO_3 in 33.21 g of 15% bis(pentamethylcyclopentadienyl)cobalt(III) hydroxide (i.e., Cp^*_2CoOH) solution, and adding 28.67 g of Bindzil 15NH3/500 silica sol (obtained from Akzo-Nobel-PQ Silica). The water and ammonia were partially removed under reduced pressure at 70°C, and the resulting gel (molar composition SiO_2 : 0.15 H_3BO_3 : 0.20 Cp^*_2CoOH : 30H_2O) was transferred to a Teflon-lined autoclave. This was then heated to 170°C for 1.5 days. Filtration and washing gave the desired borosilicate. Framework boron was substituted by aluminum as described elsewhere (10). This yielded a UTD-1 zeolite with a silicon-to-aluminum molar ratio of 80 according to elemental analysis.

Characterization

Phase purity and crystallinity were determined by conventional powder X-ray diffraction (XRD) using a Philips X'Pert (PN 3719) diffractometer (Cu$K\alpha$ radiation provided by a graphite monochromator) equipped with a variable divergence slit and working in the fixed irradiated area mode. Atomic absorption spectroscopy (AAS) and inductively coupled plasma atomic emission spectroscopy (ICP AES) were used to determine the Al and the B contents, respectively. MAS NMR spectra of the solids were recorded on a Varian VXR 400SWB spectrometer. The ^{29}Si MAS NMR spectra were recorded with a spinning rate of 5.5 kHz at 79.459 MHz with a 48° pulse length of 3.5 μs with 20 s repetition time. ^{27}Al MAS NMR spectra were recorded at 104.218 MHz with a spinning rate of 7 kHz and at a 9° pulse length of 0.5 μs with 0.5 s repetition time. ^{29}Si and ^{27}Al chemical shifts are reported relative to tetramethylsilane and $Al(H_2O)_6$, respectively. N_2 and Ar adsorption and desorption isotherms were measured at 77 and 87.3 K, respectively, using an automatic ASAP 2000 apparatus (Micromeritics). We used scanning electron microscopy (SEM) (JEOL JSM-6300 microscope) to assess crystal size and morphology.

Infrared spectra were measured with a Nicolet 710 FTIR spectrometer. Pyridine adsorption–desorption experiments used self-supported wafers (10 mg cm^{-1}). After overnight activation (at 673 K and 10^{-2} Pa) of the wafer, spectra were recorded. Subsequently, 6.5×10^2 Pa of pyridine was admitted in the vacuum IR cell, and excess pyridine was removed in vacuum by heating for 1 h at 523 and 673 K, respectively. After each of these heat treatments we cooled the wafer to room temperature and we recorded an IR spectrum. All the spectra were corrected for differences in sample weight.

TPD experiments employed a Micromeritics 2900 apparatus. A calcined sample (100 mg) was activated by heating them to 723 K for 2 h in an oxygen flow and for 2 h in argon flow. Subsequently, the samples were cooled to 450 K, and NH_3 was adsorbed. The NH_3 desorption was monitored with a quadrupole mass spectrometer (Balzers, Thermo Star GSD 300T) while the temperature of the sample was ramped at 10 K min^{-1} in helium flow.

Catalytic Experiments

n-Decane, tri-isopropylbenzene, and vacuum gas oil were cracked in an automated microactivity test unit (MAT) at 773 K. By changing the flow rate between 1 and 4 ml min^{-1} contact times between 0.1 and 0.5 min were obtained. Cyclic experiments involved the following: (a) strip the catalyst with N_2 for 20 min—reaction for 20 and 60 s time on stream for pure hydrocarbons and gas oil, respectively, and 1 bar of hydrocarbon; (b) strip with N_2 at reaction temperature (20 min, 30 ml min^{-1}); and (c) regenerate the catalyst at 793 K for 3 h with an air flow of 80 ml min^{-1}. In order to change the contact time, the catalyst-to-oil ratios were varied from 0.3 to 0.8 g g^{-1} by changing the amount of hydrocarbon fed through 0.5 g of catalyst.

The liquid fraction of the product was analyzed by gas chromatography, mass spectroscopy, and simulated distillation. The gaseous products were analyzed by gas chromatography. The solid products (coke) deposited on the catalyst during the reaction were quantified by measuring the CO_2 produced during regeneration with an on-line IR detector. Experiments were only considered valid when the mass balance indicated that more than 95% of all products were recovered.

We obtained kinetic rate constants by fitting the conversion data at different contact times with a first-order kinetic rate equation. We used these rate constants to compare the activities of the various catalysts (11).

RESULTS AND DISCUSSION

Zeolite Characterization

Highly crystalline SSZ-24, CIT-5, and UTD-1 silicates were synthesized. Transmission electron microscopy shows that SSZ-24, CIT-5, and UTD-1 consist of fibrous aggregates, 0.5 ± 0.2 μm long (Fig. 1).

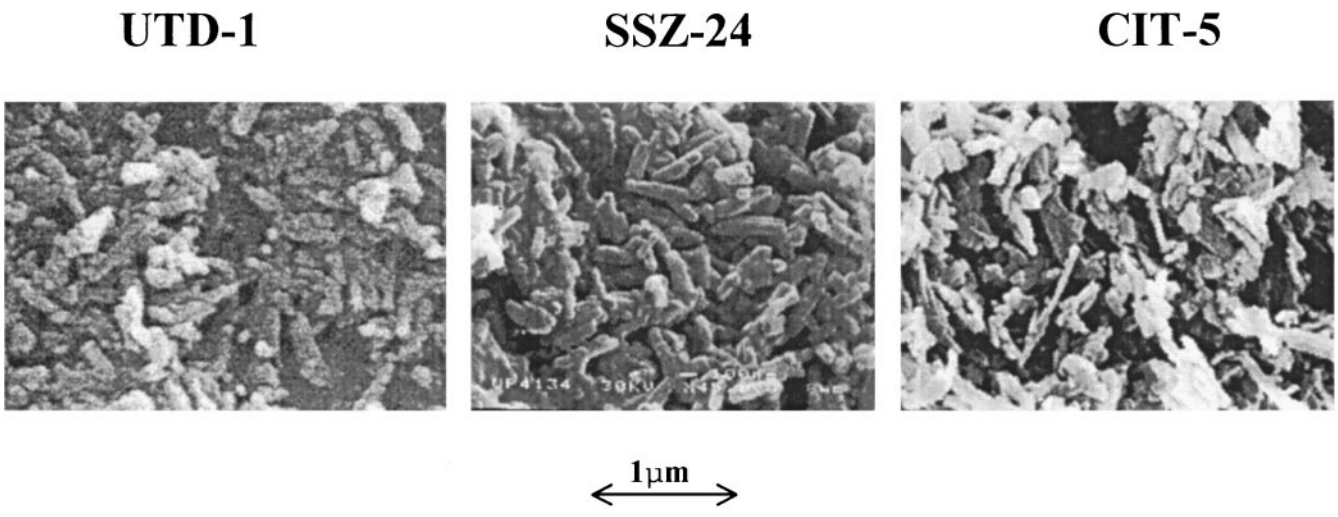

FIG. 1. Scanning electron microscopy of SSZ-24, CIT-5, and UTD-1.

Silicon-to-aluminum ratio and surface area (BET) of the three samples are shown in Table 1. The exchange procedure reported above afforded all the boron in the SSZ-24 borosilicate to be replaced by aluminum. No boron could be detected by ICP analysis after the exchange. ^{27}Al MAS NMR showed the presence of a strong peak at around 53.5 ppm, assigned to tetrahedral Al in framework positions (Fig. 2a). A small peak near −2 ppm and a broad one at higher fields may be assigned to octahedral aluminum, suggesting that a fraction of the aluminum has remained outside the framework. This nonframework alumina does not significantly affect the accessibility of the acid sites, since the micropore volume calculated from the nitrogen sorption data (using the *t*-plot method) is 0.12 cm^3/g, which agrees very well with the values reported for clean SSZ-24-type silicates (9).

The ^{27}Al MAS NMR spectrum of the as-synthesized CIT-5 zeolite only shows the presence of tetrahedral alumina at 53.3 ppm. However, after calcination the ^{27}Al MAS NMR spectrum of CIT-5 shows a small absorption at high field indicative of some nonframework aluminum. From nitrogen adsorption data we calculate that the calcined CIT-5 has a micropore volume of 0.12 cm^3/g. All silica CIT-5 has a micropore volume of 0.13 cm^3/g when it is synthesized in a fluoride medium, but of 0.11 cm^3/g when it is synthesized in a hydroxide medium (8). Accordingly, it can be safely concluded that the nonframework alumina in CIT-5 does not significantly block the pores.

^{27}Al MAS NMR spectrum (Fig. 2c) of calcined UTD-1 shows a single band at 56.0 ppm, indicating the presence of tetrahedral Al. No EFAL (band around 0 ppm) can be detected in this sample, indicating that if the calcination has removed any aluminum from the framework, this is not detectable.

Applying the Horvath–Kawazoe formalism (12) to the Ar adsorption isotherms, the mean micropore diameter was estimated to be 0.64 nm for both SSZ-24 and CIT-5. Also,

TABLE 1

Physicochemical Characteristics of Samples Used in This Study

Sample	Si/Al ratio	BET surface area ($m^2 g^{-1}$)
UTD-1	80	305
CIT-5	50	364
SSZ-24	50	293

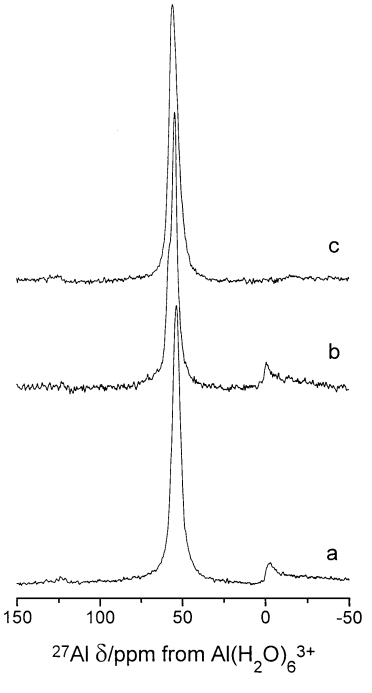

FIG. 2. ^{27}Al MAS NMR spectra of calcined (a) SSZ-24, (b) CIT-5, and (c) UTD-1.

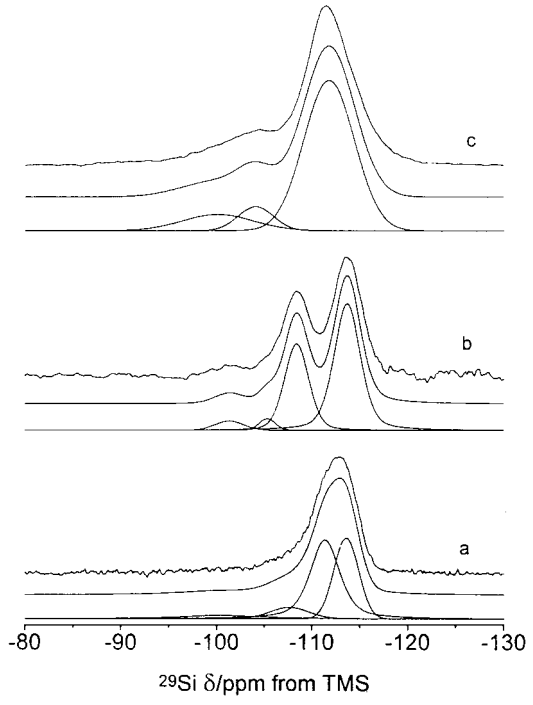

FIG. 3. ^{29}Si MAS NMR spectra of calcined (a) SSZ-24, (b) CIT-5, and (c) UTD-1.

crystallographic data suggest that the highly puckered 14 MR window in CIT-5 and the highly coplanar 12 MR window in SSZ-24 have about the same diameter (0.73 nm for SSZ-24 and 0.755×0.73 nm for CIT-5) (8). For UTD-1 we calculate a micropore diameter of 0.69 nm. This agrees with its higher crystallographic pore size (10×7.5 (7)) as compared to SSZ-24 and CIT-5.

The ^{29}Si MAS NMR spectra of calcined SSZ-24, CIT-5, and UTD-1 are shown in Figs. 3a, 3b, and 3c. All spectra show peaks at around -106 ppm (assigned to Si(3Si, 1Al)) and at around -101 ppm (assigned to Si(3Si, 1OH)), suggesting that all three materials contain framework aluminum and structural defects. The overlap of the absorption impedes the determination of the framework aluminum content from these spectra.

It is interesting to note that the ^{29}Si MAS NMR spectrum of CIT-5 shows two lines near -108 and -114 ppm, which are assigned to Si(4Si) species in different crystallographic sites. The chemical shifts of these peaks and relative intensities (3 : 5) are in good agreement with both the ^{29}Si MAS NMR spectrum of the pure silica defect-free material and the refined structure (8). In marked contrast, the shape of the peak in the Si (4Si) region of the ^{29}Si MAS NMR spectrum of SSZ-24 suggests that it is split into two peaks at -111.4 and .113.6 ppm. This would suggest that our SSZ-24 sample contains two crystallographically distinct silicon sites, which would not agree with the refined structure (13).

The IR characterization of SSZ-24 in the hydroxyl region shows (Fig. 4a), in addition to a relatively small amount of free silanols (3745 cm^{-1}), two stretching OH bands at 3605 and 3495 cm^{-1}. Both of these hydroxyls portent pyridine, indicating that they both are acidic and accessible. We assign the 3605 cm^{-1} OH stretching vibration to OH groups that point relatively unhindered into the 12 MR channel system. In order to rationalize the very low wavenumber of the second hydroxyl IR band (3495 cm^{-1}) we propose two possible assignments. In the first one, we assume that some OH bridging groups are pointing to the hexagonal channel running parallel to the 12 MR channel of SSZ-24 (Fig. 5). Then, the interaction of the protons with the oxygen of the walls or the effect of the strong electric fields present in the small channels can produce a shift of the IR band towards lower wavenumbers. However, very recent calculations showed no evidence for a direct correlation between the size of the pore and the vibrational frequency of the OH directed into that pore (14). A second possible explanation assumes that the 3495 cm^{-1} band corresponds to a proton associated to a crystallographically distinct oxygen atom. Following this hypothesis, the observed band shift could be due to the hydrogen bonding between the acidic proton and neighboring framework oxygen atoms or silanol groups at defects.

The IR spectra in the pyridine region (Fig. 6) show the presence of the pyridinium ions. Some of these remain adsorbed at temperatures as high as 673 K (Fig. 6b1). We observe only a small amount of Lewis acid sites corresponding to the interaction of pyridine with nonframework aluminum (1456 cm^{-1}). This confirms our conclusion based

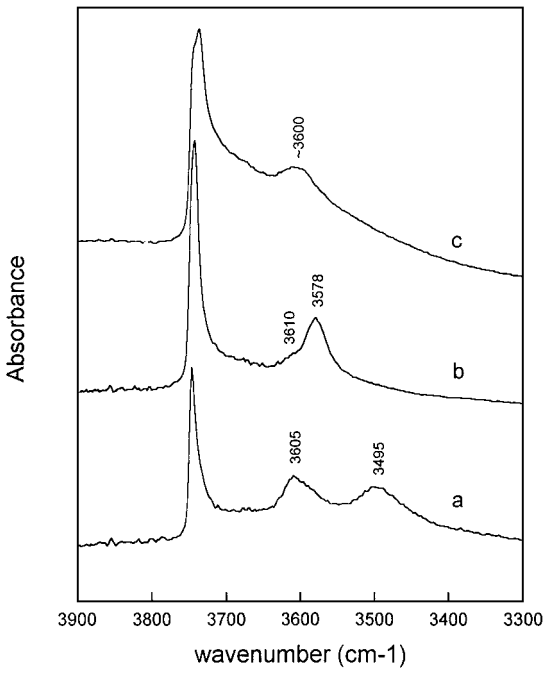

FIG. 4. Infrared spectra in the OH region of (a) SSZ-24, (b) CIT-5, and (c) UTD-1. The spectra are offset for clarity.

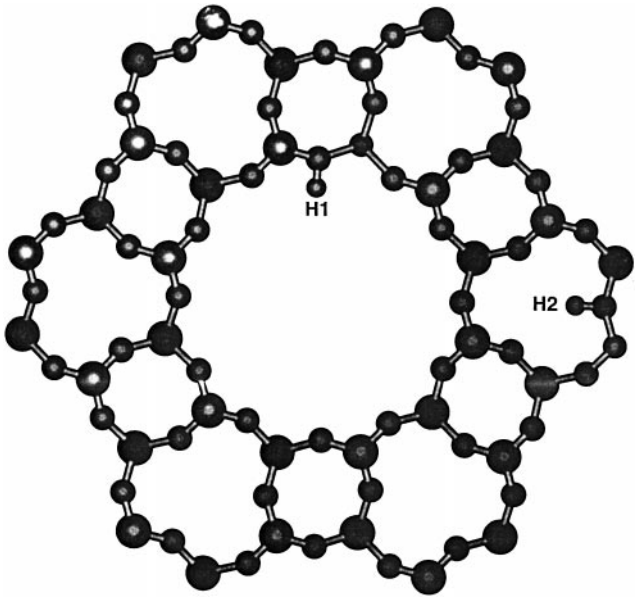

FIG. 5. Structural representation of SSZ-24 channel, showing the two possible orientations of bridging OH groups.

on ^{27}Al MAS NMR that the amount of nonframework aluminum in our silicates is small.

The OH stretch IR spectrum of the CIT-5 zeolite (Fig. 4b) shows a large number of external silanol groups (3745 cm^{-1}). The acidic hydroxyl groups at 3578 and at 3610 cm^{-1} (shoulder) are accessible and acidic enough to interact with pyridine. Following our discussion of the OH stretch spectrum of SSZ-24, we can conclude that, in the CIT-5 spectra, the small frequency difference between the two bands (~30 cm^{-1}) and its narrowness discards the possibility of hydrogen bond interactions or confinement effects. Consequently, we assign them to protons at crystallographically distinct oxygen atoms.

As observed for SSZ-24, CIT-5 contains only a few Lewis acid sites. This suggests that our CIT-5 sample contains only a little nonframework alumina and is in agreement with our interpretation of its ^{27}Al MAS NMR spectrum.

The IR spectrum of the UTD-1 sample shows a single broad OH band at ~3600 cm^{-1} assigned to acidic bridging hydroxyl groups (Fig. 4c) and an intense band at ~3500–3600 cm^{-1} assigned to internal silanol groups. All OH groups detected at ~3600 cm^{-1} can portent pyridine.

When we compare the intensities of the 1550 cm^{-1} pyridinium bands of SSZ-24 and of CIT-5 at 623 K (Figs. 6a1 and 6a2), SSZ-24 appears to contain more pyridinium ions as compared to CIT-5. Thus, SSZ-24 appears to contain a somewhat higher acid site density as compared to CIT-5. Furthermore, both zeolites have some Brønsted acid sites that are strong enough to retain pyridine at 673 K. CIT-5 contains somewhat more of these sites as compared to SSZ-24 (Figs. 6b1 and 6b2). UTD-1 forms significantly fewer pyridinium ions as compared to CIT-5 or SSZ-24 (Fig. 6a3). In agreement with its lower acid site density UTD-1 also has a lower bulk aluminum density (see Table 1). Moreover, UTD-1 does not retain any pyridine at temperatures as high as 673 K (Fig. 6b3), indicating that the acid sites in UTD-1 are less strong as compared to those in SSZ-24 and CIT-5.

In addition, we have assessed the average acid strength of the three zeolite samples with NH_3 TPD (Fig. 7). The NH_3 desorption maxima for SSZ-24, CIT-5, and UTD-1 are at 595, 623, and 610 K, respectively. This is at a significantly

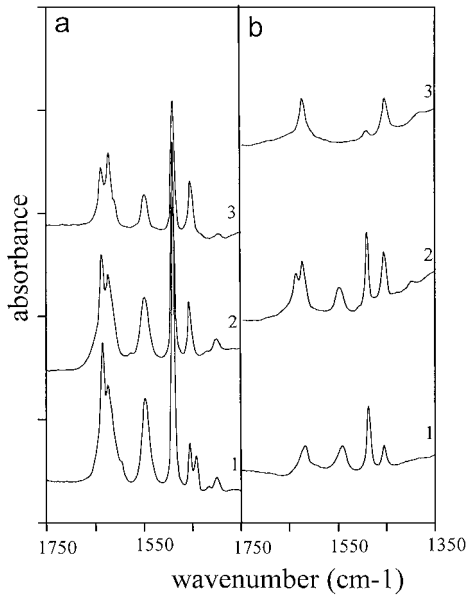

FIG. 6. IR spectra of pyridine remaining adsorbed after desorption in vacuum at (a) 523 K and (b) 673 K, for the following samples: (1) SSZ-24, (2) CIT-5, and (3) UTD-1. The spectra are offset for clarity.

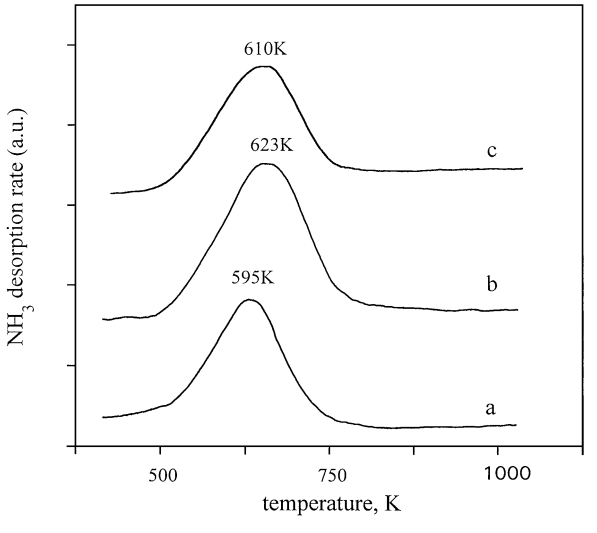

FIG. 7. Normalized NH_3 TPD of (a) SSZ-24, (b) CIT-5, and (c) UTD-1. The spectra are offset for clarity.

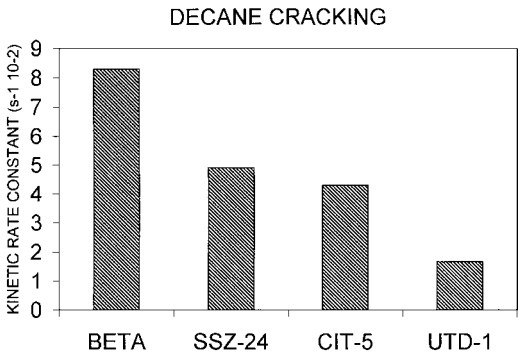

FIG. 8. First-order kinetic rate constants for *n*-decane cracking over SSZ-24, CIT-5, and UTD-1.

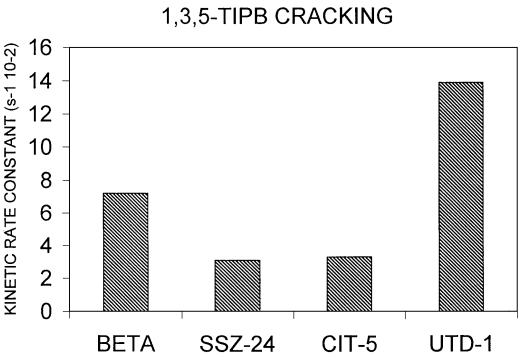

FIG. 10. First-order kinetic rate constants for 1,3,5-tri-isopropylbenzene cracking over SSZ-24, CIT-5, and UTD-1.

lower temperature as compared to mordenite and ZSM-5 with maxima at 745 and 683 K, respectively (spectra not shown), but at a temperature comparable to Y-type zeolites (Si/Al = 15–50) (maximum at ~623 K). Thus, the average strength of the Brønsted acid sites in SSZ-24, CIT-5, and UTD-1 is comparable to the strength of the sites in Y-type zeolites, but significantly less as compared to the strength of the sites in ZSM-5 and mordenite.

Catalytic Results

First we discuss the conversion of a relatively small molecule (*n*-decane) on SSZ-24, CIT-5, and UTD-1. We expect that the activity of the three zeolite samples in *n*-decane conversion will not be affected by diffusional limitations, so that the measured (intrinsic) activity will only reflect differences in Brønsted acidity. The results presented in Fig. 8 show that the activity in *n*-decane cracking is almost identical for SSZ-24 and CIT-5, whereas UTD-1 is significantly less active. These results are in good agreement with the assessments of the total Brønsted acid site densities in our IR spectroscopic study.

As a second reactant we discuss tri-isopropylbenzene. Its dimensions (Fig. 9) were calculated with the Insight II software from Biosym. According to our calculations, the flat tri-isopropylbenzene molecule can penetrate into the elliptical pores of UTD-1, but is excluded from the pores of CIT-5 and SSZ-24. Consequently, tri-isopropylbenzene will only interact with the external surface of these two zeolites.

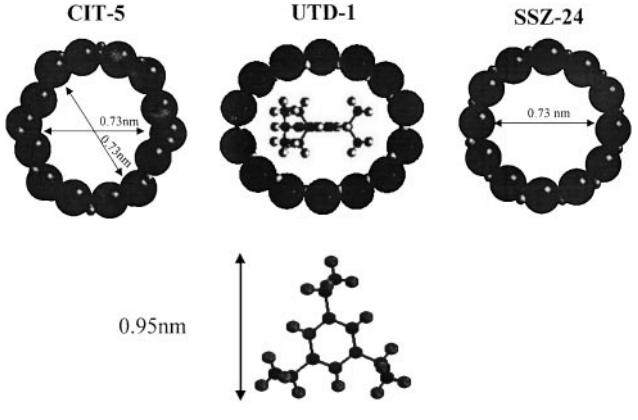

FIG. 9. Channel cross-section representation for SSZ-24, CIT-5, and UTD-1 as compared with a tri-isopropylbenzene molecule.

When we compare the kinetic rate constants determined from catalytic cracking tests (Fig. 10), CIT-5 and SSZ-24 have a similar catalytic activity in tri-isopropylbenzene conversion. This suggests that the external surfaces of these similarly sized crystals (Fig. 1) have a comparable activity. Strikingly, the activity of UTD-1 is much higher as compared to SSZ-24 and CIT-5, despite UTD-1's lower Brønsted acid site density. This confirms that only the relatively small, external surfaces of SSZ-24 and CIT-5 convert tri-isopropylbenzene, whereas in UTD-1 also the (large) internal surface is involved. Thus, the 14 MR channels in the CIT-5 zeolite offer no clear catalytic advantage in comparison to the similarly sized 12 MR channels in an SSZ-24 zeolite. Only the 14 MR channels of UTD-1 are significantly larger as compared to conventional 12 MR zeolites so as to offer a potential catalytic advantage.

To further evaluate the potential merit of the unusually large pore size of UTD-1 we compared its performance in the catalytic cracking of a complex feedstock (an Arabian light vacuum gas oil (Table 2)). This feedstock contains molecules with a rich variety of sizes and shapes and is representative of feedstock used in fluid catalytic cracking. For

TABLE 2

Characteristics of Vacuum Gas Oil

Density (g cm^{-3})	0.873	Conradson carbon (wt%)	0.03
API gravity	30.6°	MeABP (°C)	366
Nitrogen (ppm)	370	K-UOP	12.00
Sulfur	1.65	Viscosity (c.s. at 50°C)	8.249

Distillation curve (°C)

IBP	5	10	20	30	40	50	60	70	80	90	FBP
167	245	281	304	328	345	363	380	401	425	450	551

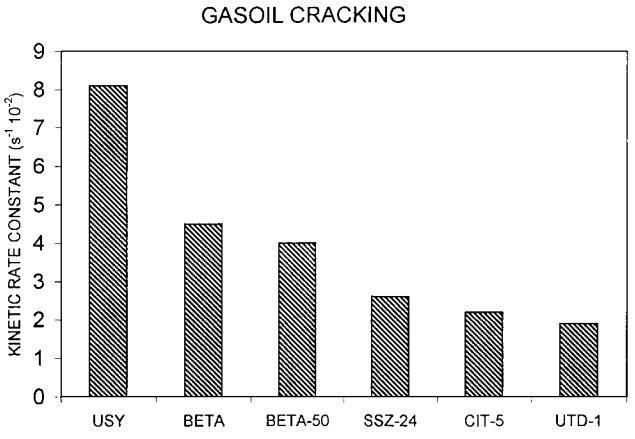

FIG. 11. Second-order kinetic rate constants for gas oil cracking over SSZ-24, CIT-5, and UTD-1.

comparison we included a USY, a Beta zeolite (Si/Al = 30), and the SSZ-24 and CIT-5 samples. The results given in Fig. 11 clearly show that the gas oil cracking activity, as quantified by the first-order kinetic rate constant, is much higher for the tridirectional USY and Beta zeolites than for any of the other three unidirectional zeolites. One may argue that the higher activity of the USY (0.84 μm) and Beta (0.1 μm) zeolites is due to a higher framework aluminum density or a smaller crystallite size (in the case of the Beta sample). Therefore, we included a Beta zeolite with a framework aluminum density comparable to that of CIT-5 and SSZ-24 (Si/Al = 50) and with a crystallite size of 0.3 μm (Beta-50 in Fig. 11). This Beta zeolite sample turns out to be still significantly more active than any of the unidirectional zeolites studied here. An explanation for the superior performance of the Beta zeolite sample could be that the diffusion of large molecules in its tridirectional pores is faster than in unidirectional 12 MR and 14 MR ring channels. In addition, the tridirectional pores in the Beta zeolite will not be blocked by coke as easily as unidirectional pore zeolites, so that the Beta zeolite is likely to effectively convert vacuum gas oil for a longer period of time as compared to the unidirectional zeolites. Apparently, the extra-large pore size of UTD-1 is still limited to converting the largest molecules present in the vacuum gas oil feed and, furthermore, does not improve its resistance to coke formation. Thus, extra-large unidirectional zeolites are of limited interest for fluid catalytic cracking, but could be of interest for processes where coke formation is limited such as *n*-paraffin dehydrocyclyzation, hydroisomerization–hydrocracking, or even naphthalene alkylation.

CONCLUSIONS

We have shown here that CIT-5 and SSZ-24 zeolites have two distinct types of acidic OH groups, whereas UTD-1 has only one type. We detected a few sites with an enhanced Brønsted acid strength in our CIT-5 and SSZ-24 zeolite samples, but none in our UTD-1 sample. Overall, the strength of the Brønsted acid sites in CIT-5, SSZ-24, and UTD-1 was less as compared to the strength of the sites in Mordenite or ZSM-5.

According to our detailed analysis of our CIT-5 and SSZ-24 zeolite samples, both samples have a comparable acid site density, acid site strength distribution, and crystal size. Accordingly, the CIT-5 and the SSZ-24 zeolites have a very similar catalytic performance.

Large, flat organic molecules such as tri-isopropylbenzene can be converted inside the large ellipsoidal pores of UTD-1. These molecules cannot enter the smaller, circular pores of CIT-5 and SSZ-24.

In a microactivity test with an industrial fluid catalytic cracking feedstock (a vacuum gas oil), the performance of the ultra-large unidirectional pores of UTD-1 is inferior to that of tridirectional 12 MR zeolites such as USY or Beta. We speculate that UTD-1 could be better suited for processes like the dehydrocyclization of paraffins or the alkylation of substituted naphthalene.

ACKNOWLEDGMENTS

The authors thank Dr. M. T. Blasco for NMR measurements and useful discussions. We acknowledge the financial support by the Spanish CICYT (Project MAT97-0723 and Project MAT97-1016-C02-01).

REFERENCES

1. Corma, A., *Chem. Rev.* **95**, 559 (1995).
2. Kubota, Y., and Davis, M. E., *Mater. Res. Soc. Symp. Proc.* **435**, 263 (1996).
3. Esterman, M., McCusker, L. B., Baerlocher, Ch., Merrouche, A., and Kessler, H., *Nature* **352**, 320 (1991).
4. Moore, P. B., and Shen, J., *Nature* **306**, 356 (1983).
5. Balkus, K. J., Jr., Gabrielov, A. G., and Saudler, N., *Mater. Res. Soc. Symp. Proc.* **368**, 359 (1995).
6. Wagner, P., Yoshikawa, M., Lovallo, M., Tsuji, K., Tasptsis, M., and Davis, M. E., *Chem. Commun.*, 2179 (1997); Yoshikawa, M., Wagner, P., Lovallo, M., Tsuji, K., Takewaki, T., Chen, C. Y., Beck, L. W., Jones, Ch., Tsapatsis, M., Zones, S. I., and Davis, M. E., *J. Phys. Chem. B.* **102**, 7139 (1998).
7. Freyhardt, C. C., Tspatsis, M., Lobo, R. F., Balkus, K. J., and Davis, M. E., *Nature* **352**, 320 (1991).
8. Barret, P. A., Diaz-Cabañas, M. J., Camblor, M. A., and Jones, R. H., *J. Chem. Soc. Faraday Trans.* **24**, 2475 (1998).
9. Lobo, R. F., and Davis, M. E., *Microporous Mater.* **3**, 61 (1994).
10. Zones, S. I., and Chen, C. Y., WO97/46486 (1997).
11. Corma, A., Fornés, V., Forni, L., Marquez, F., Martinez-Triguero, J., and Moscotti, D., *J. Catal.*, in press.
12. Horwath, G., and Kawazoe, K., *J. Chem. Eng. Jpn.* **16**, 470 (1983).
13. Bialek, R., Meier, W. M., Davis, M. E., and Annen, M. J., *Zeolites* **11**, 438 (1991).
14. Sastre, G., and Lewis, D. W., *J. Chem. Soc. Faraday Trans.* **94**, 3049 (1998).